Characterization and Application of Nanomaterials (2023) Volume 6 Issue 1
doi: 10.24294/can.v6i1.3183

ORIGINAL RESEARCH ARTICLE

Green synthesis and characterization of iron nanoparticle using extracted bitter guard leaves used as methylene blue removal

Thin Phyu Lin[1], Kyu Kyu Khaing[1], Aung Than Htwe[1,2,*], May Thazin Oo[1], Su Su Soe Nyunt[1]

[1] *Department of Chemistry, Mohnyin University, Mohnyin 01162, Kachin State, Myanmar. E-mail: aungthanhtwe76@gmail.com*

[2] *Department of Chemistry, University of Yangon, Kamaryut 11041, Myanmar.*

ABSTRACT

Zero-valent iron is a moderately reducing reagent that is both non-toxic and affordable. In the present work, iron nanoparticles were synthesized using bitter guard leaf extract (*Momordica charantia* L.) (BGL-Fe NP). Using leaf samples from bitter protectant extract, iron nanoparticles were synthesized with secondary metabolites such as flavonoids and polyphenols acting as capping and reducing agents. Polyphenols reduce Fe^{2+}/Fe^{3+} to nanovalent iron or iron nanoparticles. Iron nanoparticles were synthesized by reducing iron chloride as a precursor with bitter protective leaf extract in an alkaline environment. The obtained BGL-Fe NPs were calcined for 4 h at various temperatures of 400 °C, 500 °C, and 600 °C. The obtained samples were coded as BGL-Fe NPs-4, BGL-Fe NPs-5, and BGL-Fe NPs-6, respectively. The synthesized BGL-Fe NPs were systematically characterized by XRD, SEM, FTIR, UV-Vis and TG-DTA analysis. The obtained BGL-Fe NPs were then used as an adsorbent to remove the aqueous solution of basic methylene blue (MB) dye. MB concentration was monitored using UV-Vis spectroscopy.

Keywords: Iron Nanoparticle; Characterization; Methylene Blue

ARTICLE INFO

Received: 4 May 2023
Accepted: 20 May 2023
Available online: 4 June 2023

1. Introduction

Momordica charantia L., a member of the Cucurbitaceae family, is also known as bitter guard. Simple or alternating leaves measure 4–10 cm long and have 3–6 deeply divided lobes. Tendrils can be unbranched or branched. Fruit has an irregular dehiscence as a fleshy capsule or is indehiscent. It is ovoidal, elliptical, or spindle-shaped, packed with flat seeds in pulp, typically with a ridged surface. The fruits are green when they are young and become orange or yellow as they ripen.

Numerous studies have reported on the environmentally friendly production of iron nanoparticles using a variety of plant extracts. Iron nanoparticles (Fe NPs) have mostly been biosynthesised utilizing the extract of green tea, a readily available and affordable resource. Making use of green tea (Camellia sinensis) extract, which contains a number of polyphenols, Hoag *et al*.[1] synthesized nZVI. The stable nanoparticles were created at room temperature without the use of a surfactant or polymer. Plant polyphenols function as capping and reducing agents, producing stable, green, zero-valent iron particles with special characteristics.

According to Ghanim *et al*.[2], dye pollutants are one of the primary sources of environmental contamination in a wide range of sectors. There are several ways to clean up wastewater from all industries, in-

cluding textile industry effluent. Adsorption is the most often used technique among them since it is efficient and easy to apply[3,4].

In this study, bitter guard leave extracts were successfully used to prepare iron nanoparticles (BGL-Fe NPs). Polyphenols from bitter guard have been found to have capping and reducing properties. It designed an entirely novel synthetic method for sorbent here using green chemistry principles and eco-friendly, cost-effective, non-hazardous, and renewable materials. Modern methods, including XRD, FTIR, UV-visible, SEM, and TG-DTA, were used to analyze the properties of the prepared BGL-Fe NPs. Finally, the main objective of this study is to reveal the efficient adsorptive removal of organic waste, such as the cationic synthetic dye methylene blue, by the synthesized BGL-Fe NPs sorbent.

2. Materials and methodology

2.1 Collection and extraction

The leaves of bitter guard (*Momordica charantia* L.) were collected from Nammar Township, Kachin State, Myanmar, in December 2022. The samples were cut into small pieces and dried in the shade at room temperature for one week. The dried leaves samples were ground with a grinder and stored in airtight bottles.

2.2 Preparation of iron nanoparticle (BGL-Fe NPs)

The iron nanoparticles (BGL-Fe NPs) were prepared by the co-precipitation method. Extracts were prepared by heating 20 g of bitter guard leaves powder in 200 mL of distilled water for 30 min at 85 °C on a hot plate. The extract was filtered using filter paper. $FeCl_3 \cdot 6H_2O$ (3.381 g) was dissolved in 250 mL of distilled water and stirred continuously to obtain a 0.1 M Fe(III) solution. The bitter guard leave extract was mixed into a 0.1 M Fe(III) solution for 15 min. The color immediately changed after the addition of bitter guard leaves extract to the ferric chloride solution. And then, sodium hydroxide (1M) solution was added drop by drop into the iron(III) mixture solution, which was carried out with constant stirring at 80 ºC until the solution reached pH 8. The color of the solution was changed from brown to reddish-brown. The solution was continuously stirred at 80 °C for 2 h. Then, the solution was centrifuged at 3,000 rpm for 5 min. The synthesized BGL-Fe NPs were washed several times with distilled water until neutral (pH 7) to remove any alkali metals. The obtained neutral BGL-Fe NPs were washed again with ethanol and dried for 3 h in the oven at 80 °C. After that, the dried BGL-Fe NPs were calcinied in a muffle furnace at 400 °C, 500 °C, and 600 °C for 4 h to achieve stable BGL-Fe NPs. This sample was coded BGL-Fe NPs-4 for 400 °C, BGL-Fe NPs-5 for 500 °C, and BGL-Fe NPs-6 for 600 °C. All samples were crushed with a motor and pestle and sieved with a 40-mesh sieve. Finally, the sample was stored in a sealed bottle and placed in a dessicator for further use. The schematic diagram was described in **Figure 1**.

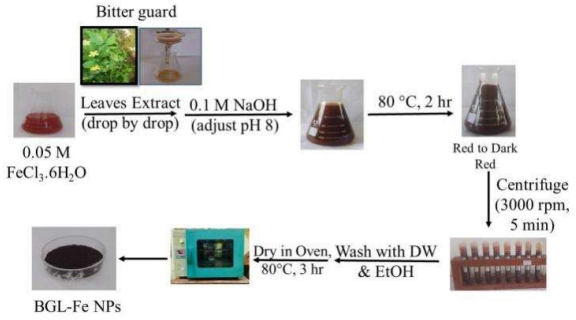

Figure 1. Schematic diagram of preparation of iron nanoparticle (BGL-Fe NPs) using bitter guard extract.

2.3 Characterization of iron nanoparticle (BGL-Fe NPs)

Green synthesized iron nanoparticles are characterized through different techniques such as XRD, FTIR, SEM, UV-Vis, and TG-DTA to elucidate their properties. X-ray diffraction studies were used to determine the prepared powdered samples (varistors) with the help of Rigaku Multiflux X-ray diffractometer with Cu Kα (λ = 1.5418 Å) monochromatic radiation. The powdered samples were scanned from 10° to 80° with a scanned speed of 0.01°/sec. The applied voltage and current of the X-ray diffractometer were set to be 50 kV and 40 mA. The identification of functional groups was investigated by FT-IR with a

Perkin Elmer spectrum of 2,000. The analyses were carried out in the range of 400 cm^{-1}–4,000 cm^{-1}. Nanoparticles powder samples (varistors) were characterized with the assistance of (JEOL, Model No. JSM-5610 LV). Applied voltage and current of SEM were set to be 15 kV, 68 uA, and 94X magnification.

2.4 Adsorption experiment

Adsorption by the batch technique was used to study methylene blue (MB) removal using BGL-Fe NPs. First, the accurate MB amount was dissolved in deionized water to make stock solutions of MB at a concentration of 50 mg/L. Then, the stock solutions were taken for dilution to make a daily solution. At 25 °C, different adsorbent volumes were mixed with 25 mL of MB solution in 100 mL Erlenmeyer flasks. The concentration of the solution, contact time, pH of the solution, and adsorbent dose are a few important parameters that affect the removal of MB. All concentrations of MB in aqueous solutions were analyzed by the ultraviolet-visible (UV-Vis) method at 668 nm using a GENESYS 10S (Thermo Scientific) UV-Vis spectrometer.

$$\text{removal efficiency (\%)} = \frac{C_i - C_f}{C_i} \times 100\ \% \qquad (1)$$

where C_i and C_f are the initial and final concentrations of MB (mg/L).

3. Results and discussion

3.1 Characterization

The identity of the synthesized iron nanoparticles was established using the following analytical techniques:

3.1.1 XRD analysis

The X-ray diffractogram of the synthesized BGL-Fe NPs, BGL-Fe NPs-4, BGL-Fe NPs-5, and BGL-Fe NPs-6 (**Figure 2**) shows the presence of characteristic peaks at 2θ values of 30.17° and 57.34° corresponding to hematite (α-Fe_2O_3), whereas the peak at 35.45° corresponds to magnetite (Fe_3O_4). In addition, the peaks at 28.50° correspond to Geothite (α-FeOOH) whereas a peak at 45.32° and 62.89° correspond to zerovalent iron (α-Fe) phases. It is therefore confirmed that Fe NPs-JF contain zero-valent iron nanoparticles (nZVI) along with iron oxides and oxyhydroxide[5,6]. Using Scherrer's formula, which is provided below, and the peak broadening profile of the peak at all 2θ values, the average crystallite size was estimated using the FWHM value of the most intense peak.

$$d = \frac{0.94\lambda}{\beta\cos\theta}$$

where λ is the wavelength (1.5418 Å) and β is the full width at half maximum (FWHM) of the corresponding peak[7]. The average crystallite size of synthesized BGL-Fe NPs calculated from Sherrer's equation was 47.66 nm for BGL-Fe NPs, 10.55 nm for BGL-Fe NPs-4, 11.33 nm for BGL-Fe NPs-5, 15.72 nm for BGL-Fe NPs-6, respectively.

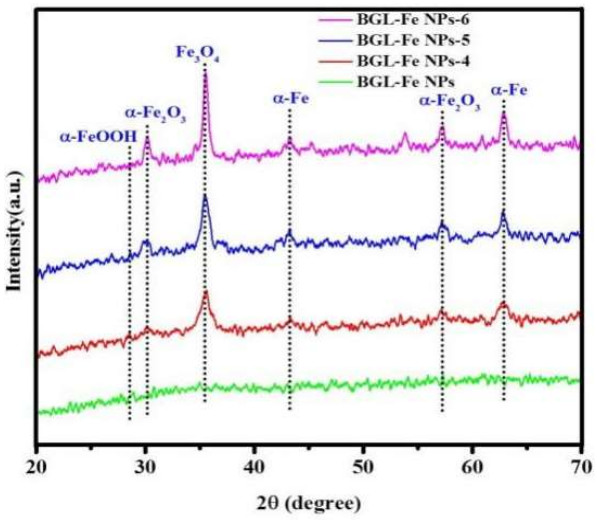

Figure 2. XRD pattern of BGL-Fe NPs before and after calcination temperature.

3.1.2 FTIR analysis

The potential extract functionalities that may have been the cause of the EDX-found carbon signature were determined using FTIR analysis. Several peaks were observed in the range of 1,000–3,400 cm^{-1}. In **Figure 3**, the iron nanoparticles correspond to the vibrations of the Fe-O bonds. The bands at 3,021 cm^{-1}, 1,636 cm^{-1}, 1,440 cm^{-1}, 870 cm^{-1}, and 540 cm^{-1} were confirmed as OH, C=C, aliphatic C-H bending, C-H bending, FeO stretching. The absorption bands at around 540 cm^{-1} attributed to the FeO symmetrical

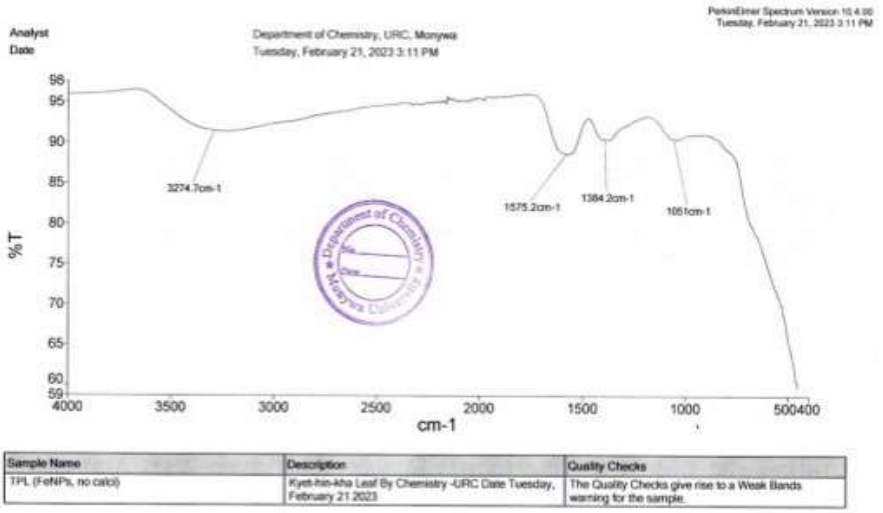

Sample Name	Description	Quality Checks
TPL (FeNPs, no calci)	Kyet-hin-kha Leaf By Chemistry -URC Date Tuesday, February 21 2023	The Quality Checks give rise to a Weak Bands warning for the sample.

(A)

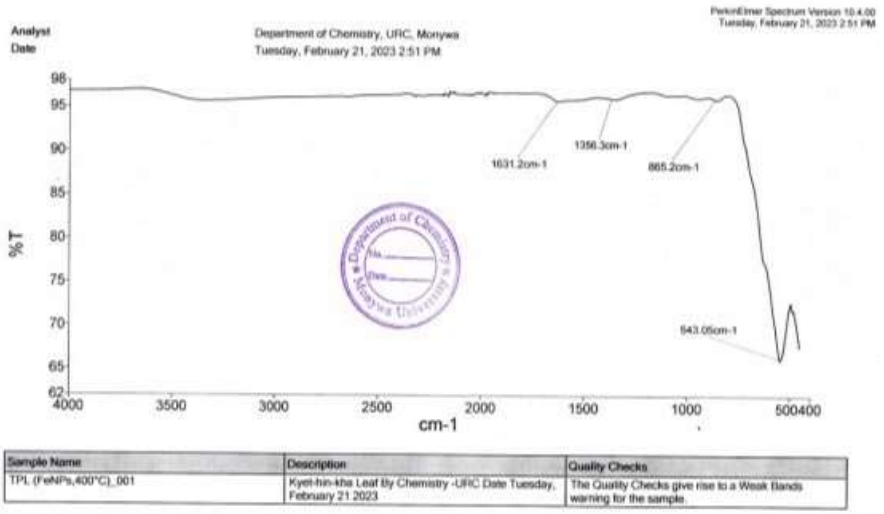

Sample Name	Description	Quality Checks
TPL (FeNPs,400°C)_001	Kyet-hin-kha Leaf By Chemistry -URC Date Tuesday, February 21 2023	The Quality Checks give rise to a Weak Bands warning for the sample.

(B)

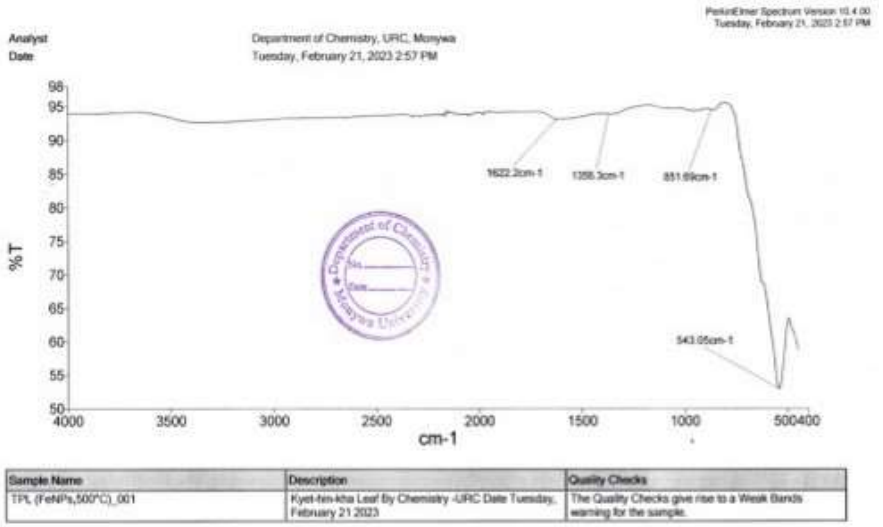

Sample Name	Description	Quality Checks
TPL (FeNPs,500°C)_001	Kyet-hin-kha Leaf By Chemistry -URC Date Tuesday, February 21 2023	The Quality Checks give rise to a Weak Bands warning for the sample.

(C)

Figure 3. *Continued.*

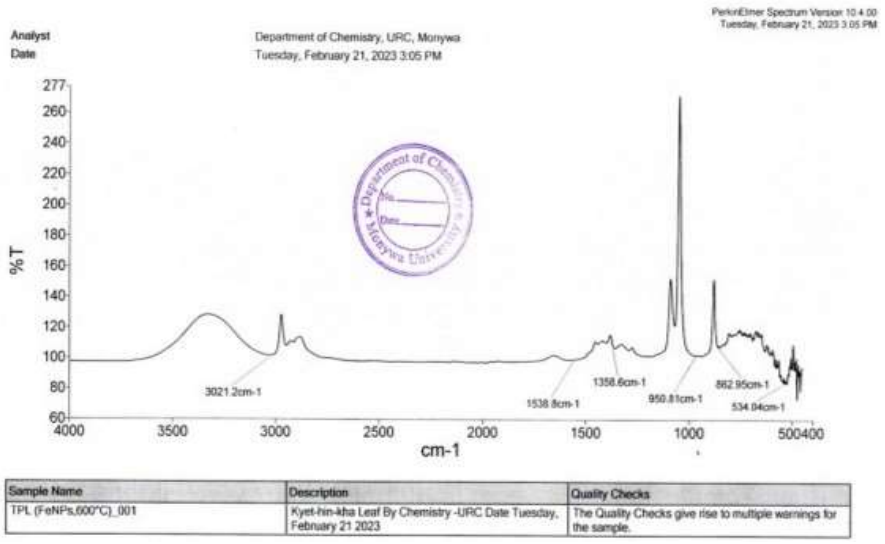

(D)

Figure 3. FTIR spectra data of **(A)** BGL-Fe NPs; **(B)** BGL-Fe NPs-4; **(C)** BGL-Fe NPs-5; and **(D)** BGL-Fe NPs-6.

stretching. The highest peaks at 3,359–3,361 cm^{-1} correspond to polyphenols, showing the greater abundance and noticeable presence of phenolic functional groups for the reduction of Fe^{3+} to Fe^{0}. Other than that, the more available phenolic groups provide a favorable molecular arrangement for the delocalization of unpaired electrons. So, the leaf extract captured the property of successful scavenging of free radicals. The appearance of a peak at 3,359 cm^{-1} and a shift to 3,361 cm^{-1} indicate that the phenolic or amine groups of the leaves extract may be involved in the formation of Fe NPs. It can be concluded from the spectra that the polyphenols in the leaves extract were responsible for the reduction and stabilization of Fe NPs, which also agrees with the UV-visible analysis[7].

3.1.3 SEM analysis

The morphology and diameter distribution of BGL-Fe NPs are determined by SEM. The SEM images of BGL-Fe NPs are shown in **Figure 4(A)–(D)** at 10 kV acceleration voltage and 94x magnification. Analysis of SEM images of all nanoparticles of BGL-Fe NPs shows that the nanoparticles are agglomerated and tend to form irregular spherical particles on the surface. Aggregated nanoparticles have been shown to have rough surfaces. Iron nanoparticles are in close contact with each other due to the magnetic properties of iron species. This may be due to the presence of different polyphenols in the leaves extract, which can significantly affect the final morphology and size of iron nanoparticles.

In **Figure 5(A)–(D)**, size diameter distributions were evaluated by measuring at least 200 particles from SEM micrograph. The results are obtained that the average diameters of the prepared nanoparticles are 12.11 µm for BGL-Fe NPs, 12.23 µm for BGL-Fe NPs-4, 16.59 µm for BGL-Fe NPs-5, and 12.53 µm for BGL-Fe NPs-6, respectively. According to the size diameter distribution histograms, the significant size of BGL-Fe NPs-5 increased among the samples. It indicates that the produced BGL-Fe NPs possess a narrow size distribution.

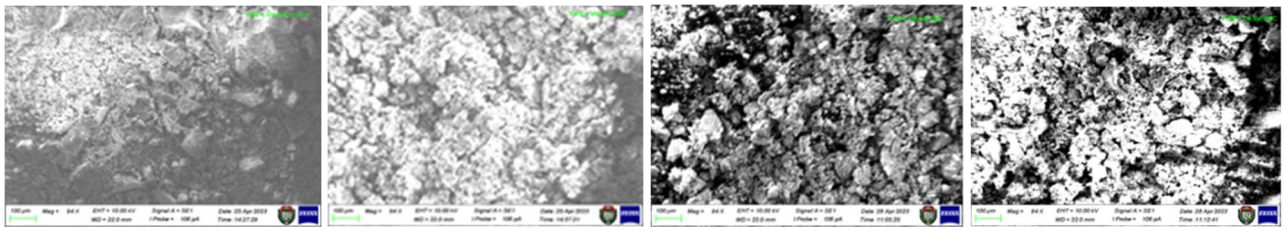

Figure 4. SEM spectra data of **(A)** BGL-Fe NPs; **(B)** BGL-Fe NPs-4; **(C)** BGL-Fe NPs-5; and **(D)** BGL-Fe NPs-6 and Particle size diameter distribution.

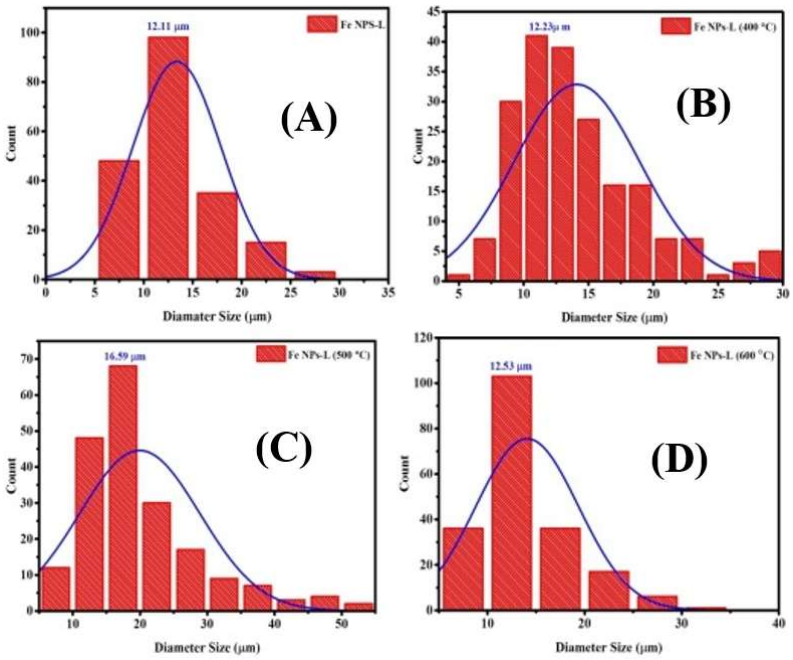

Figure 5. Particle size diameter distribution of **(A)** BGL-Fe NPs; **(B)** BGL-Fe NPs-4; **(C)** BGL-Fe NPs-5; and **(D)** BGL-Fe NPs-6.

3.1.4 UV-Vis analysis

UV-vis absorption spectra of iron nanoparticles are represented in **Figure 6**. As seen in **Figure 6**, the absorption spectra of BGL-Fe NPs nanoparticle peaks were detected at 229 nm and 274 nm for BGL-Fe NPs, 264 nm for BGL-Fe NPs-4, 263 nm for BGL-Fe NPs-5, and 361 nm for BGL-Fe NPs-6, respectively. Therefore, a sharp and relatively narrow absorption between about 229 nm was observed. The absorption spectrum of bitter guard α–Fe^0 showed a maximum in the range of 216–300 nm, which is identical to the characteristic absorption peak for the reported metallic iron[8].

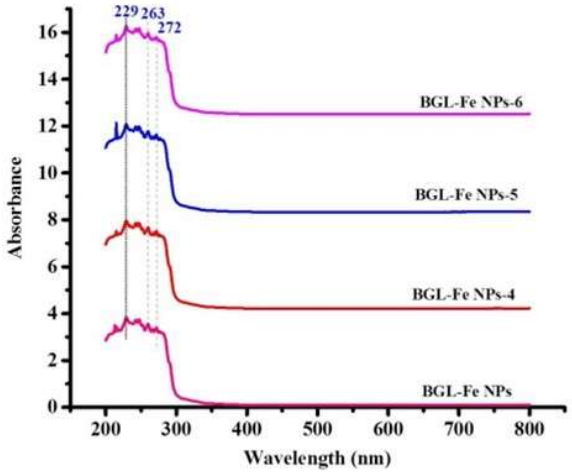

Figure 6. UV-visible absorbance spectra of BGL-Fe NPs using leaves extract.

As seen in **Figure 7**, BGL-Fe NPs samples give an optical band gap value that shows 4.03 eV for BGL-Fe NPs, 3.98 eV for BGL-Fe NPs-4, 3.83 eV for BGL-Fe NPs-5, and 3.70 eV for BGL-Fe NPs-6, respectively. Due to charge transitions, the absorption decreases and the optical band gap increases. The BGL-Fe NPs prepared in this study are expected to be more useful in photonic and electronic devices.

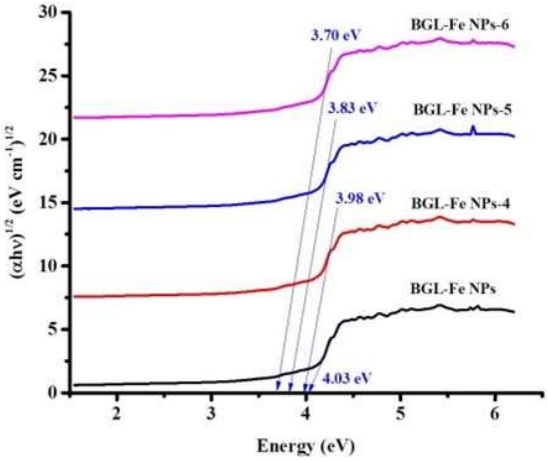

Figure 7. Plots of hν Vs $(\alpha h\nu)^{1/2}$ of BGL-Fe NPs using leaves extract.

3.1.5 TG-DTA analysis

The thermogram profiles of the prepared BGL-Fe NPs samples are shown in **Figure 8**. The thermogram of BGL-Fe NP samples exhibits three

stages of noticeable weight loss between 37 °C and 600 °C. The first stage in the temperature range is 37.09 °C to 230 °C, with 20.42% weight loss for BGL-Fe NPs. There is a loss of moisture. In the second stage, the temperature range between 230 °C and 300 °C was observed to cause 10.15% of weight loss for BGL-Fe NPs. This is due to the dehydration of water molecules. One exothermic peak was seen at 291.30 °C in both samples. The third stage is the loss in weight of 2.28% for BGL-Fe NPs, which was observed to take place within the temperature range of 300 °C to 600 °C due to the combustion of some residue.

The thermogram of BGL-Fe NPs-4, BGL-Fe NPs-5, and BGL-Fe NPs-6 samples in **Figure** 8 shows one phase of weight loss between 38 °C and 300 °C. In this temperature range, it was found that the weight loss of 4.14% for BGL-Fe NPs-4, 1.54% for BGL-Fe NPs-5, and 1.47% for BGL-Fe NPs-6, respectively. In this stage, weight loss may be loss of surface water or OH groups adsorbed on the surface of the iron oxide. The broad endothermic peak was observed between 53 °C and 73 °C. This occurrence is due to the oxidation product of FeO.

According to the TGDTA analysis, it was demonstrated that there is no appreciable weight loss at 300 °C above, indicating that the prepared samples are thermally stable.

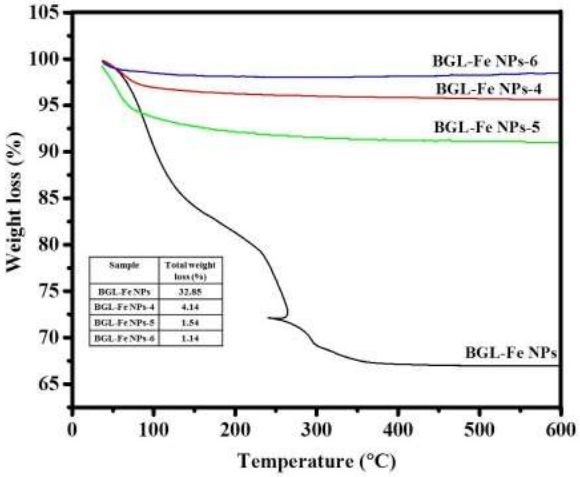

Figure 8. TG-DTA thermogram of Fe NPs-L.

3.2 Investigation of the removal percent of methylene blue by iron nanoparticles

3.2.1 Effect of concentration

The effect of color concentration of methylene blue dye solution on the adsorption of BGL-Fe NPs, BGL-Fe NPs-4, BGL-Fe NPs-5, and BGL-Fe NPs-6 was studied under the optimized conditions of time and dosage of adsorbents. The concentrations varied from 50 to 250 ppm. **Figure 9** showed that the effect of the initial concentration of methylene blue (MB) solution on the adsorption of BGL-Fe NPs, BGL-Fe NPs-4, BGL-Fe NPs-5, and BGL-Fe NPs-6. According to **Figure 9**, it was found that the percent removal was decreased from about 97.52% to 62.73% for all iron nanoparticles. These indicated that the initial MB concentration of Fe BGL-Fe NPs-6 was more effective than that of BGL-Fe NPs. Higher the removal percentages were observed for lower concentrations of MB for BGL-Fe NPs-6.

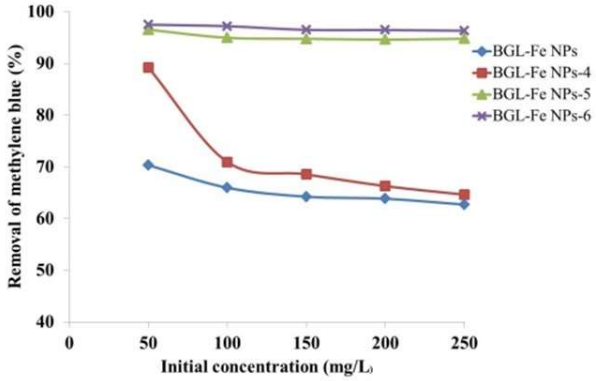

Figure 9. Effect of the initial concentration on the MB sorption process depending on the phase contact time 3 h: BGL-Fe NPs (dosage 0.4 g, pH 7, shaking speed 250 rpm, temperature 25 °C).

3.2.2 Effect of pH

Figure 10 shows that the lowest removal efficiency of 78.154% of BGL-Fe NPs, BGL-Fe NPs-4, BGL-Fe NPs-5, and BGL-Fe NPs-6 was recorded at pH = 5 (highly acidic medium). At low pH values, the presence of excess H^+ ions on the surface of Fe NPs can compete with the MB cations for adsorption sites, causing an electrostatic repulsion[9]. A further increase in pH from 5 to 9 resulted in an enhancement of MB removal efficiency from 78.154% to 81.186% for Fe NPs-L (400 °C) and from 80.092% to 82.982% for Fe NPs-F (500 °C). The increase in negatively charged sites (due to OH^-) resulting in electrostatic attraction and compounds with the cationic dye

may be responsible for the finding[10]. An increase in pH value from 5 to 9 resulted in a decrease in MB removal efficiency from 81.16% to 78.154% of BGL-Fe NPs, and 81.468% to 80.092% in BGL-Fe NPs-4, respectively. This result may be due to the corrosion or hydrolysis of Fe^0 in alkaline solutions (e.g., pH around 10), leading to the production of iron ions and ferric iron precipitated as iron oxide/hydroxide[11]. These reactions can be described by the following equations (Equations (2)–(4)):

$$Fe^0 \rightarrow Fe^{2+} + 2\bar{e} \quad (2)$$

$$2Fe^0 + O_2 + 2H_2O \rightarrow 2Fe^{2+} + 4OH^- \quad (3)$$

$$Fe^0 + H_2O \rightarrow Fe^{2+} + H_2 + 2OH^- \quad (4)$$

The corrosive results of the BGL-Fe NPs formation might cover the surface of the nanoparticles, which hindered electron transport from Fe0 to MB[12]; as a result, the adsorption process slowed down. Similar to this, Fan *et al.*[13] showed that dye removal by BGL-Fe NPs particles was inefficient under excessively basic or acidic conditions but performed in a mildly acidic range. According to Sun *et al.*[11], the net surface charge of n BGL-Fe NPs particles turned positive when the solution pH was lower than the point of zero charge (pH_{ZPC}) of 8.0, which attracted the anionic dye. On the other hand, the adsorbent surface becomes negatively charged when the solution pH approaches pH_{ZPC}, which strengthens the attraction mechanism with cations.

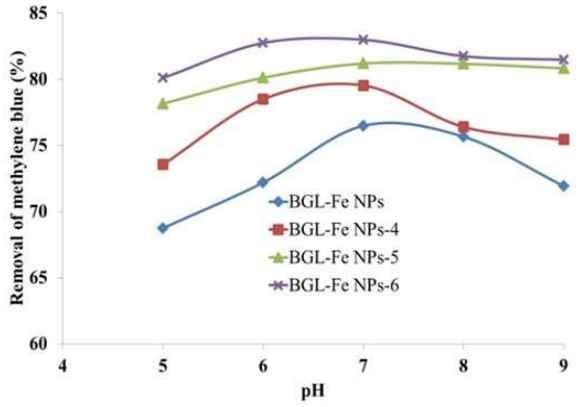

Figure 10. Effect of pH on the MB sorption process depending on the phase contact time 3 h: BGL-Fe NPs (dosage 0.4 g, initial concentration 50 ppm, shaking speed 250 rpm, temperature 25 °C).

3.2.3 Effect of dosage

The efficiency of BGL-Fe NPs, BGL-Fe NPs-4, BGL-Fe NPs-5, and BGL-Fe NPs-6 sorbents in removing MB from a 50 ppm MB solution was determined by monitoring the contact time. In the investigations, the color intensities of aliquots were spectrophotometrically measured at specified times using a batch approach. The dosage, as seen in **Figure 11**, varied from 0.1 to 0.5 g. The proportion of each adsorbent decreased after 0.4 g, but during the 3 h period, BGL-Fe NPs-6 sorbent removed the highest MB among BGL-Fe NPs, BGL-Fe NPs-4, and BGL-Fe NPs-5 sorbents.

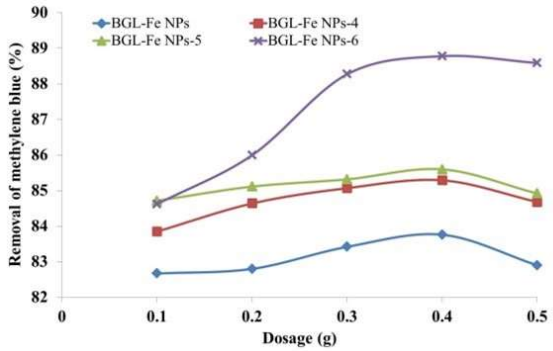

Figure 11. Effect of dosage on the MB sorption process depending on the phase contact time 3 h: BGL-Fe NPs (initial concentration 50 ppm, pH 7, shaking speed 250 rpm, temperature 25 °C).

3.2.4 Effect of time

The MB removal efficiency of BGL-Fe NPs, BGL-Fe NPs-4, BGL-Fe NPs-5, and BGL-Fe NPs-6 sorbents was tested against 50 ppm ferric chloride solution by measuring the contact time. The experiments were performed using the batch method, where the color intensity of the aliquots was monitored spectrophotometrically at certain time intervals. **Figure 12** showed that the time varied from 1 to 5 h. From **Figure 12**, it has been observed that the maximum removal of MB dye was achieved at 3 h of reaction with 81.82% BGL-Fe NPs, BGL-Fe NPs-4, BGL-Fe NPs-5, and BGL-Fe NPs-6. From the results, it can be observed that there was decreased in the percentage of each adsorbent after 3 h, whereas BGL-Fe NPs-6 sorbent was more removal percent of MB than Fe NPs sorbent for investigation time periods.

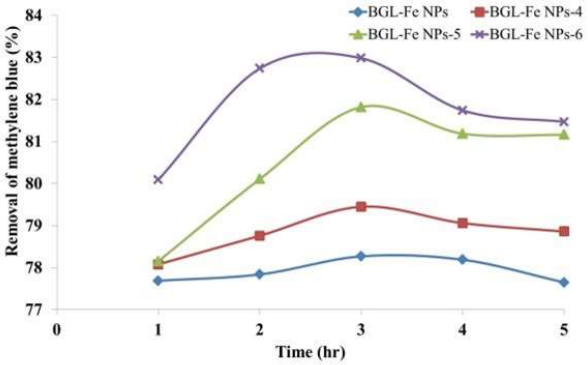

Figure 12. Effect of contact time on the MB sorption process of BGL-Fe NPs (dosage 0.4 g, initial concentration 50 ppm, pH 7, shaking speed 250 rpm, temperature 25 °C).

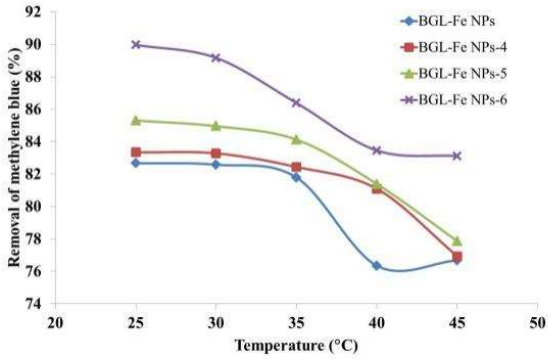

Figure 13. Effect of contact time on the MB sorption process of BGL-Fe NPs (dosage 0.4 g, initial concentration 50 ppm, pH 7, shaking speed 250 rpm, temperature 25 °C).

3.2.5 Effect of temperature

Temperature plays an important role in influencing the removal efficiency of a MB adsorption process of Fe NPs. The effect of reaction temperature (25, 30, 35, 40 and 45 °C) on the removal efficiency using Fe NPs is described in **Figure 13**. Here, the efficiency of BGL-Fe NPs-4 for MB removal was 98.96, 89.16, 86.38, 81.38, and 77.86% at 25, 30, 35, 40, and 45 °C. It is shown that the removal of MB from BGL-Fe NPs-4 was an endothermic process. However, the MB removal efficiency of BGL-Fe NPs at 25, 30, 35, 40, and 45 °C was 85.30, 84.95, 84.12, 83.45, and 83.11%. It was suggested that BGL-Fe NPs were less effective than BGL-Fe NPs-6 in removing the MB because the surface of BGL-Fe NP-6 was more covered by iron oxide and iron hydroxide. Thus, the removal efficiency can be improved by increasing the temperature because it promotes the collisions of MB molecules, which in turn leads to more activation energy[14]. Increasing the solution temperature can improve the adsorption efficiency[15,16]: (a) increases the solubility and mobility of MB in the solution, which increases the intra-particle diffusion; (b) reduce the amount of dissolved oxygen in the solution, prevent the oxidation of iron nanoparticles; (c) increase the activation energy, create new adsorption sites, and form a complex reaction surface; and (d) facilitates the production of a swelling effect within the internal structure of the absorbent, which facilitates the penetration of molecules into the pores[17].

4. Conclusion

In this research, iron nanoparticles synthesized from aqueous bitter guard leave extracts were characterized by modern methods such as XRD, FTIR, SEM, UV-Vis, and TG-DTA. Iron nanoparticles rich in iron oxide/oxhydroxide can be easily prepared using aqueous extracts of bitter guard leaves as reducing and capping agents at different calcination temperatures of 400, 500, and 600 °C for 4 h. Particle morphology and size were investigated using SEM and XRD techniques. SEM microscopy of all prepared Fe NPs showed agglomerated clusters. The crystallite size of BGL-Fe NPs was observed to vary from 10.55 nm to 47.66 nm before and after annealing temperature. FT IR measurements confirmed the attachment of compounds in the extract to iron nanoparticles. Functional groups of phenolic compounds can contribute to the formation of metal nanoparticles. From the FT IR spectral data of all BGL-Fe NPs, a strong stretching absorption band of the Fe-O bond at 543.05 cm^{-1} was observed. According to the results, the functional groups successfully synthesized BGL-Fe NPs.

The product of BGL-Fe NPs was confirmed by change of colour and the UV-Vis spectra surface Plasmon resonance center at 229 nm. From UV-visible data, the band edge-absorption peak of all Fe NPs is found to be between about 229 nm and 247 nm, and the band gap values are in the range of 4.06 eV to 4.28 eV for Fe NPs-L with changes the calcination temperature. The absorption decreases, and the optical band gap increases due to charge transfer transitions.

In TG-DTA thermogram, the total weight loss (%) shows about 32.85% in BGL-Fe NPs before calcination. After calcination, the total weight loss changes in the range between 4.14% and 1.14% for BGL-Fe NPs (400 °C, 500 °C, and 600 °C). It is found that the total weight loss of BGL-Fe NPs after calcination is lower than that of BGL-Fe NPs before calcination. TG-DTA analysis demonstrated that there is no appreciable weight loss at 300 °C above, indicating that all Fe NPs samples are thermally stable.

The prepared BGL-Fe NPs showed promising prospects for MB removal. The removal efficiency was found to depend on the test conditions. The optimum removal occurred at pH 7 and 25 °C with 0.4 g Fe NP. In addition, the removal efficiency increased rapidly after 1 h and then increased more slowly, followed by an equilibrium period after 3 h. The removal percentage of BGL-Fe NPs prepared by methylene blue indicator was about 81.18% to 96.53% of the BGL-Fe NPs sample.

This study provides convincing evidence that stabilized nanoparticles of BGL-Fe NPs can be used to remove MB from a cationic dye solution, potentially leading to an innovative treatment method that is likely to be more cost-effective and less disruptive to the environment.

Author contributions

Conceptualization, TPL and ATH; methodology, TPL; software, ATH; validation, KKK, MTO and SSSN; formal analysis, TPL; investigation, TPL; resources, TPL; data curation, ATH; writing—original draft preparation, MTO, SSSN and ATH; writing—review and editing, ATH; visualization, MTO and KKK; supervision, ATH; project administration, ATH; funding acquisition, ATH. All authors have read and agreed to the published version of the manuscript.

Conflict of interest

The authors declare no conflict of interest.

Acknowledgments

The authors gratefully acknowledged to Professor Nyein Nyein Htwe, Head of the Department of Chemistry, Mohnyin University, Myanmar for her encouragement and administrative supervision beginning from this research work. We would like to express my special thanks Myinzu Minn, Rector, Mohnyin University, Myanmar who gave us the opportunity to do this research.

References

1. Hoag GE, Collins JB, Holcomb JL, *et al*. Degradation of bromothymol blue by 'greener'nanoscale zero-valent iron synthesized using tea polyphenols. Journal of Materials Chemistry 2009; 19(45): 8671–8677. doi: 10.1039/B909148C.
2. Ghanim D, Al-Kindi GY, Hassan AK. Green synthesis of iron nanoparticles using black tea leaves extract as adsorbent for removing eriochrome blue-black B dye. Engineering and Technology Journal 2020; 38(10): 1558–1569. doi: 10.30684/etj.v38i10A.1225.
3. Prema P, Thangapandian S, Selvarani M, *et al*. Color removal efficiency of dyes using nanozerovalent iron treatment. Toxicological & Environmental Chemistry 2011; 93(10): 1908–1917. doi: 10.1080/02772248.2011.606613.
4. Tan KB, Vakili M, Horri BA, *et al*. Adsorption of dyes by nanomaterials: Recent developments and adsorption mechanisms. Separation and Purification Technology 2015; 150: 229–242. doi: 10.1016/j.seppur.2015.07.009.
5. Kuang Y, Wang Q, Chen Z, *et al*. Heterogeneous fenton-like oxidation of monochlorobenzene using green synthesis of iron nanoparticles. Journal of Colloid and Interface Science 2013; 15(410): 67–73. doi: 10.1016/j.jcis.2013.08.020.
6. Wu Y, Zeng S, Wang F, *et al*. Heterogeneous Fenton-like oxidation of malachite green by iron-based nanoparticles synthesized by tea extract as a catalyst. Separation and Purification Technology 2015; 154: 161–167. doi: 10.1016/j.seppur.2015.09.022.
7. Sravanthi M, Manjunatha KG. Corrosion studies of as casted and heat treated aluminium-7075 composites. Materials Today: Proceedings 2018; 5(10): 22581–22594. doi: 10.1016/j.matpr.2018.06.632.
8. Bolade OP, Williams AB, Benson NU. Green synthesis of iron-based nanomaterials for environmental remediation: A review. Environmental Nanotechnology, Monitoring & Management 2020; 13: 100279. doi: 10.1016/j.enmm.2019.100279.
9. Gouamid M, Ouahrani MR, Bensaci MB. Adsorption equilibrium, kinetics and thermodynamics of

methylene blue from aqueous solutions using date palm leaves. Energy Procedia 2013; 36: 898–907. doi: 10.1016/j.egypro.2013.07.103.
10. Albadarin AB, Collins MN, Naushad M, *et al*. Activated lignin-chitosan extruded blends for efficient adsorption of methylene blue. Chemical Engineering Journal 2017; 307: 264–272. doi: 10.1016/j.cej.2016.08.089.
11. Sun X, Kurokawa T, Suzuki M, *et al*. Removal of cationic dye methylene blue by zero-valent iron: Effects of pH and dissolved oxygen on removal mechanisms. Journal of Environmental Science and Health, Part A 2015; 50(10): 1057–1071. doi: 10.1080/10934529.2015.1038181.
12. Khan A, Prabhu SM, Park J, *et al*. Azo dye decolorization by ZVI under circum-neutral pH conditions and the characterization of ZVI corrosion products. Journal of Industrial and Engineering Chemistry 2017; 47: 86–93. doi: 10.1016/j.jiec.2016.11.017.
13. Fan J, Guo Y, Wang J, *et al*. Rapid decolorization of azo dye methyl orange in aqueous solution by nanoscale zerovalent iron particles. Journal of Hazardous Materials 2009; 166(2–3): 904–910. doi: 10.1016/j.jhazmat.2008.11.091.
14. Lin Y, Chen Z, Chen Z, *et al*. Decoloration of acid violet red B by bentonite-supported nanoscale zero-valent iron: Reactivity, characterization, kinetics and reaction pathway. Applied Clay Science 2014; 93–94: 56–61. doi: 10.1016/j.clay.2014.02.020.
15. Bao Y, Zhang G. Study of adsorption characteristics of methylene blue onto activated carbon made by Salix psammophila. Energy Procedia 2012; 16: 1141–1146. doi: 10.1016/j.egypro.2012.01.182.
16. Chen Z, Wang T, Jin X, *et al*. Multifunctional kaolinite-supported nanoscale zero-valent iron used for the adsorption and degradation of crystal violet in aqueous solution. Journal of Colloid and Interface Science 2013; 398: 59–66. doi: 10.1016/j.jcis.2013.02.020.
17. Hamdy A, Mostafa MK, Nasr M. Zero-valent iron nanoparticles for methylene blue removal from aqueous solutions and textile wastewater treatment, with cost estimation. Water Science and Technology 2018; 78(2): 367–378. doi: 10.2166/wst.2018.306.